

Mechanical response of agar gel irradiated with Nd:YAG nanosecond laser pulses.

Francisco G. Pérez-Gutiérrez¹, Rodger Evans²
Santiago Camacho-López², Guillermo Aguilar¹

1. Department of Mechanical Engineering, University of California, Riverside; 900 University Ave, Riverside, CA, USA 92521.
2. Departamento de Óptica, Centro de Investigación Científica y de Educación Superior de Ensenada; Km. 107 Carretera Tijuana - Ensenada C.P. 22860, Ensenada, B.C., México.

ABSTRACT

Nanosecond long laser pulses are used in medical applications where precise tissue ablation with minimal thermal and mechanical collateral damage is required. When a laser pulse is incident on a material, optical energy will be absorbed by a combination of linear and nonlinear absorption according to both: laser light intensity and material properties. In the case of water or gels, the first results in heat generation and thermoelastic expansion; while the second results in an expanding plasma formation that launches a shock wave and a cavitation/boiling bubble. Plasma formation due to nonlinear absorption of nanosecond laser pulses is originated by a combination of multiphoton ionization and thermionic emission of free electrons, which is enhanced when the material has high linear absorption coefficient. In this work, we present measurements of pressure transients originated when 6 ns laser pulses are incident on agar gels with varying linear absorption coefficient, mechanical properties and irradiation geometry using laser radiant exposures above threshold for bubble formation. The underlying hypothesis is that pressure transients are composed of the superposition of both: shock wave originated by hot expanding plasma resulting from nonlinear absorption of optical energy and, thermoelastic expansion originated by heat generation due to linear absorption of optical energy. The objective of this work is to evaluate the relative contribution of each absorption mechanism to mechanical effects in agar gel. Real time pressure transients are recorded with PVDF piezoelectric sensors and time-resolved imaging from 50 μm to 10 mm away from focal point.

Keywords: Nanosecond laser pulses, artificial tissue models, linear and nonlinear absorption, pressure waves.

1. INTRODUCTION

Laser-ablation of tissue with nanosecond laser pulses has been widely studied in the past and has been introduced in medical applications^{1, 2}. The mechanisms of interaction between nanosecond laser pulses and biological tissues are very interesting for medical applications because it is possible to induce tissue ablation with high precision and minimal thermal and mechanical damage in the surrounding tissue. At low irradiance, the optical energy is coupled to a material according to the material's linear absorption coefficient. In this regime, thermal effects are dominant and if the laser pulse is shorter than the acoustic relaxation time, stress confinement conditions occur and a thermoelastic expansion of the material launches a pressure wave.

In addition, at high irradiance, it is possible to couple optical energy to a transparent material at low irradiance. As the irradiance increases, the laser pulse ionizes the material via multiphoton ionization seeding free electrons that serve as absorbers for photons. When photons are absorbed further, more electrons are released serving as absorbers for more photons via avalanche ionization². When a nanosecond laser pulse is tightly focused in the bulk of transparent water and/or gel, plasma formation launches a shock wave and an oscillating bubble; these phenomena have been widely studied in the past with time resolution of a few nanoseconds³.

In this work, we present results of experiments carried out to characterize mechanical effects in artificial tissue models irradiated with nanosecond laser pulses. The variables studied in this work include the geometry of laser exposures, mechanical and optical properties of agar gel.

Agar gels are excellent artificial tissue models because of its high water content. In addition, its mechanical properties can be varied changing the agar concentration, and its optical properties can also be varied adding dyes and intralipids to change absorption and scattering coefficients respectively. The result is a more realistic tissue model compared with simple water, which has been used in several studies before⁴. Addition of external agents, like dyes and intralipids, not only changes the linear absorption coefficient, but also inevitably changes the nonlinear absorption coefficient which results in differences in threshold fluence for optical breakdown⁵. Experiments were carried out with two different geometrical configurations, two agar gel concentrations and three different dye concentrations. In our experiments we included water to compare our results with gel.

Mechanical effects were characterized using home made polyvinylidene fluoride (PVDF) transducers. This type of transducers is suitable for the experiment proposed because of its low cost, fast time response and high sensitivity. However, the disadvantage for the current experimental conditions in the laboratory is that pressure can only be measured at approximately 1 mm away from the beam focus position without risk of damaging the transducer. In order to measure pressure within a few tens of micrometers from the laser beam position, a time-resolved imaging (TRI) system was developed. Images from TRI system provide information of the rate of change of the shock wave radius as a function of time, i.e. the shock wave velocity. A mathematical model combines the shock wave velocity, the material properties and speed of sound to calculate pressure difference between the shocked and unshocked regions. The combination of both, the PVDF sensors and the TRI system allows us to characterize the pressure distribution within the tissue model used in one dimension.

Finally, a brief discussion about the pressure signal obtained with the PVDF sensors with both laser exposure configurations and the effect of varying the linear absorption coefficient is presented.

2. MATERIALS AND METHODS

2.1 Agar gels

Agar gel is an excellent artificial tissue model because its high water content makes its thermal properties very similar to that of tissue. In addition, it is possible to change its mechanical properties varying the agar concentration and its optical properties can be adjusted adding dyes. For the experiments presented here, agar gel blocks with thickness from 1 to 11 mm were made. The agar concentrations were 2 and 4 grams of agar powder in 100 ml of deionized water. To prepare the gels, deionized water was heated to boiling point and agar powder in solution was added to meet the mentioned concentrations; then the liquid agar gel was poured into molds of the appropriate thickness made with glass slides. The linear absorption coefficient of the agar gels was varied adding Direct Red dye so the resulting linear absorption coefficients were 33, 47 and 97 cm^{-1} . The agar gels' linear absorption coefficient was determined according to the methodology in⁶.

2.2 Piezoelectric sensors

A polyvinylidene fluoride (PVDF) is a polymer with pyroelectric and piezoelectric properties that make it suitable to measure laser-induced stresses. A PVDF sensor was made using a 25 μm thick, aluminum-metalized PVDF film. The sensor was connected to a digital oscilloscope through a $1\text{M}\Omega$ impedance to ensure proportionality of voltage to pressure. The PVDF transducer sensitivity was 85 mV/MPa and the response time was measured to be 30 ns. Single

oscilloscope traces were obtained for each laser exposure, i.e. the signals obtained were not averaged using the oscilloscope controls.

2.3 Laser exposures and laser parameters

Figure 1 shows the configurations under which laser exposures were carried out. Fig. 1A shows the experimental set up for the measurements with the PVDF sensor. Fig. 1B shows the configuration when the beam waist was positioned on the surface of the agar gel block and Fig. 1C when the beam waist was positioned 1 mm below the agar gel block surface. The agar gel block was displaced after each laser exposure to avoid any interference with irregularities in the material due to remaining bubbles/craters from previous exposures. For experiments with water, a cuvette was glued to the sensor's aluminum case; of course it was not necessary to displace the cuvette for laser exposures in water. The beam waist was found using the equivalent target plane (ETP) system described in section 2.4 (see below).

Laser energies used in the present study were kept below 1 mJ as higher energies tend to produce long lasting bubbles⁷. The laser was focused to a beam waist $1/e^2$ radius of 2.3 μm , measured with the ETP system.

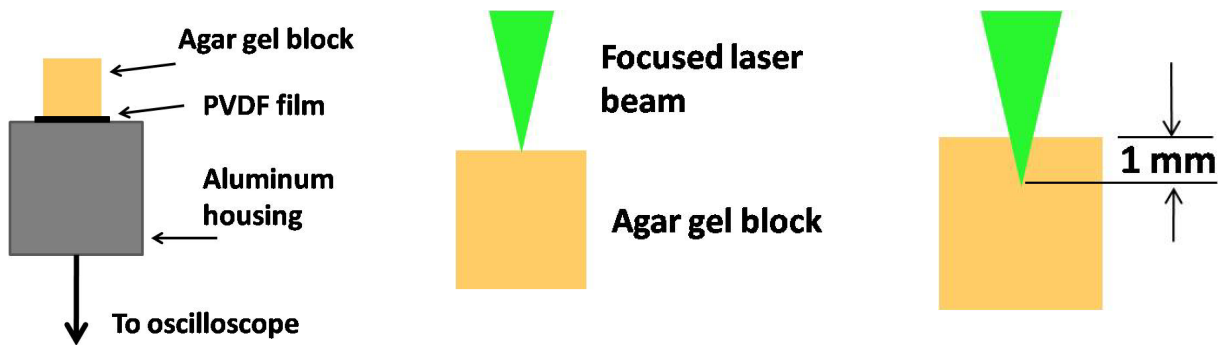


Fig. 1A. Experimental set-up for measurement of pressure transients with PVDF sensors.

Fig. 1B. Laser exposure configuration when the beam waist was positioned on the surface of the agar gel.

Fig. 1C. Laser exposure configuration when the beam waist was positioned 1 mm below the surface of the agar gel.

2.4 Time Resolved Imaging (TRI)

The experimental setup for time-resolved imaging of laser-agar gel interaction is shown in Fig. 2. It consists of two nanosecond laser systems electronically synchronized. The first, used as the pump, was a Brilliant (Quantel, Les Ulis Cedex, France), Q-switched, Nd:YAG laser that incorporates the second harmonic crystal to produce 6 ns laser pulses at $\lambda=532$ nm. The second, used as the probe, was an EKSPLA (Lithuania), Q-switched, Nd:YAG that incorporates an Optical Parametric Oscillator (OPO). The OPO was set to operate at $\lambda=1064$ nm. This probe wavelength was chosen because Direct Red dye has low linear absorption at this wavelength compared to that at 532 nm⁸.

Both beams were brought co-linear onto the sample. The delivered energy was varied with the combination of the half wave plate (HWP1) and polarizer (P1). Energy was monitored with a cross-calibrated energy meter (EM) (Ophir) to a second energy meter, (Moletron, Portland OR) positioned at the sample's location. The probe beam energy was varied changing the relative delay of the Q-switch to flash lamp by means of the triggering electronic pulse from the delay generator (DG) (BNC, San Rafael CA, USA). The beam passed collimated through the sample by means of lenses L1 ($f=35\text{mm}$) and L2 ($f=6\text{mm}$). A magnified image of the sample is formed by the combination of lenses L3 ($f=25$ mm) and L4 ($f=400$ mm) onto a CCD camera (IMI Tech, Seoul, Korea). A long-pass filter with cut-off wavelength at $\lambda=610$ nm (RF) positioned in front of the CCD blocked scattered light from the green pump beam.

The electronic delay generator DG provided the electronic pulses required to externally trigger both laser systems at 10 Hz repetition rate. The relative delay between the probe pulse and the pump pulse can be set directly with the DG unit's controls. Single laser pulses from the pump beam are selectively released by a mechanical shutter (MS) (Uniblitz, Rochester NY, USA) that opens its aperture for 100 ms, therefore allowing only one laser pulse pass through it. This is achieved by applying 3 V, 100 ms long square pulses from a signal generator SG (BNC, San Rafael CA, USA) to the mechanical shutter driver MSD (Uniblitz, Rochester NY, USA). The settings in the SG are 3 V, 5 Hz, 50% duty cycle. Simultaneously, the signal out of the SG is divided and also sent to trigger the CCD whose exposure time was set to 130 ms. This exposure time guarantees that only light from the probe pulse is captured by the CCD up to tens of milliseconds after the pump pulse released from the MS. At the same time the SG is externally triggered with a DC power supply DCPS (Circuit Specialists, Inc., Mesa AZ, USA) and a custom made hand trigger HT. The delay generator could produce delays as short as 1 ns, however the experimental setup time resolution is given by the probe pulse duration, which was 6 ns.

The lens L1 in the IR beam also served a second purpose. The CCD could be placed to have the pump beam retro-reflected from the target onto the CCD in an image relay; this setup is commonly referred as an equivalent target plane (ETP) system. The ETP was used to set the location of the beam focus in the sample when each new sample was placed. The pump laser was focused to a beam waist $1/e^2$ radius of $2.3 \mu\text{m}$, measured with the ETP system. The probe laser passed the sample with a $1/e^2$ radius of $175 \mu\text{m}$ and a per pulse energy of $1 \mu\text{J}$.

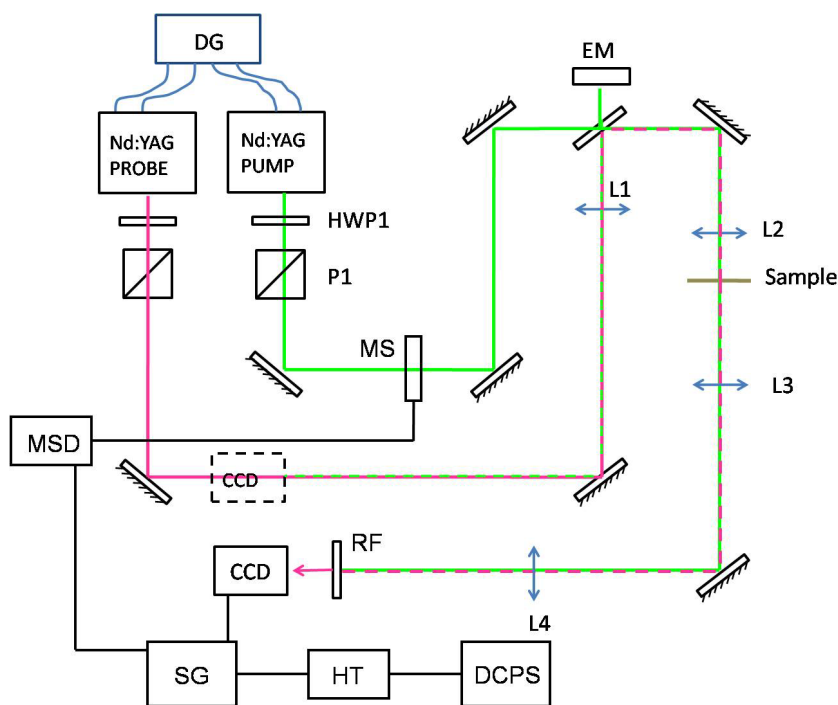


Fig. 2. Experimental set up for time-resolved imaging (TRI) and equivalent target plane (ETP) system (see body of the text).

3. RESULTS AND DISCUSSION

3.1 Variation of mechanical properties

Figure 3A shows the typical waveform obtained when a nanosecond laser pulse is focused 1 mm below the surface of the transparent agar gel blocks and deionized water. From now on, laser beam waist is in this same position unless otherwise indicated. The laser energy was $500 \pm 50 \mu\text{J}$ and the distance from the beam waist to the sensor was 10 mm. Waveforms are shown at this distance from the beam waist to ensure that the pressure wave curvature, which initially is a spheric shock wave⁹, is large enough so it can be considered as a plane wave when interacting with the PVDF film. In general the waveforms have a bipolar shape. At time $t=0$, there is a sharp rise of the signal that gets to a maximum within a few hundreds of nanoseconds and gradually decreases. It has been shown previously by optical means that the actual shock wave width produced by a 200 mJ nanosecond laser pulse in water is about 25 ns ⁹, so the actual shock waves in these experiments are most likely shorter. As the signal gradually decreases, it finds a sharp decrease until it gets to a minimum and gets to a zero value again. The sharp rise is produced by the lower part of the spherical shock wave that propagates downwards to the sensor. The sharp decrease is produced because the upper part of the shock wave that propagates upwards is reflected backwards with inverted sign when it interacts with the agar gel surface because of the acoustic impedance mismatch between the agar gel or water and the air.

Figure 3B shows the maximum amplitude of the waveforms as a function of the laser pulse energy for the three materials studied. As expected the higher the energy, the higher the amplitude. However for laser energies below $500 \mu\text{J}$, the amplitude for the 2% agar and deionized water overlap, while the amplitude for the 4% agar remains lower. This observation is more evident in Fig 3A (read below) when the amplitude of the pressure wave is measured at different distances from the beam waist. This is because 4% agar is significantly stiffer than 2% agar and deionized water; therefore the expanding plasma launches a weaker shockwave.

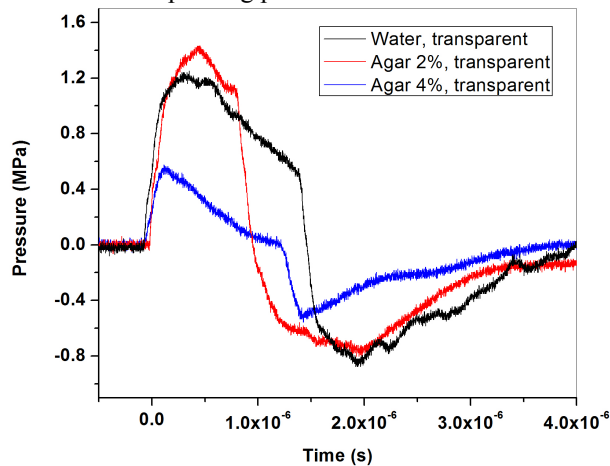


Fig. 3A. Pressure signal detected with PVDF sensor when the beam waist was positioned 1 mm below the surface of the agar gel and 10 mm away from the PVDF sensor.

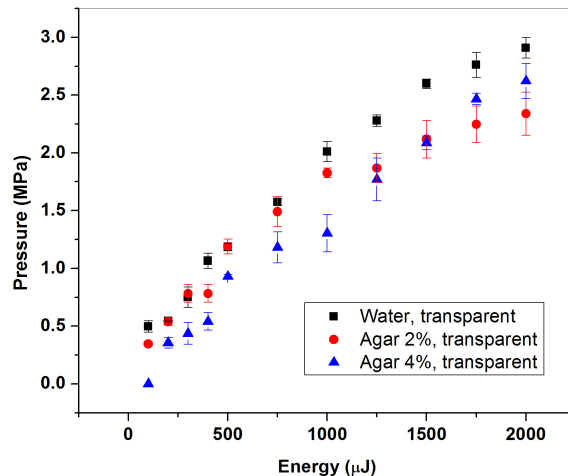


Fig. 3B. Pressure amplitude measured 10 mm away from the beam waist as a function of energy. Beam waist was positioned 1 mm below the surface of the agar gel.

3.2 Pressure as a function of distance

Figure 4A shows the maximum amplitude of the pressure wave measured at different distances from the beam waist using the agar blocks made of different thicknesses. The energy per pulse was $500 \pm 50 \mu\text{J}$. The pressure amplitude for the 2% agar blocks and deionized water overlap and show a linear decay with propagation distance from the

laser beam waist; the pressure amplitude drops by 25% while it propagates from 1 mm to 10 mm away from its origin at the beam waist to the PVDF sensor. In contrast, the maximum pressure amplitude for the 4% agar gel blocks is approximately 40% lower than that for 2% agar blocks and water. Although the amplitude for this agar concentration is higher measured 1 mm away from the beam waist, the rest of the measurements for longer distances away from the beam waist do not show decay as steep as it is for the 2% agar gel blocks and deionized water.

It is very difficult to perform measurements with the PVDF sensor at a distance shorter than 1 mm away from the beam waist because there is a large chance of damaging the sensor. Therefore, the shock wave amplitude is investigated indirectly using a mathematical model that involves the information that can be obtained from TRI. Such information is the shock wave radius as a function of the relative delay from the pump and probe pulses. The shock wave velocity can be obtained calculating the derivative of this function and plugged into equation 1. Mathematical derivation of this equation starting from mass and momentum conservation equations and Hugonit equation is in ⁸ and references therein:

$$P_1 - P_2 = \rho_2 U \left(\frac{U - C_0}{S} \right) \quad (1)$$

Where $P_1 - P_2$ is the pressure difference between the shocked and unshocked regions, ρ_2 is the agar gel density, U is the shock wave velocity, C_0 is the speed of sound and S is the Hugonit coefficient for 10% gel. C_0 and S values are 1520 m/s and 2.0 respectively⁸.

Figure 4B shows the pressure distribution inside the agar gel blocks and deionized water from 50 μm to 10 mm away from the beam waist. It contains the same data points than Figure 4A from 1 to 10 mm, in addition to the data points 50 μm away from the beam waist calculated with equation 1. Shock wave velocities for these data points were obtained from TRI. Only one data point for each material was calculated. The reason is because the field of view of the CCD camera was such that the shock wave radius increased linearly with respect to the pump-probe delay, and therefore shock wave speed was observed to be constant; in other words, it was impossible to see the shock wave deceleration until it becomes a pressure wave. It is expected that the shock wave becomes a pressure wave propagating a sonic speed in less than 150 ns after optical breakdown⁹.

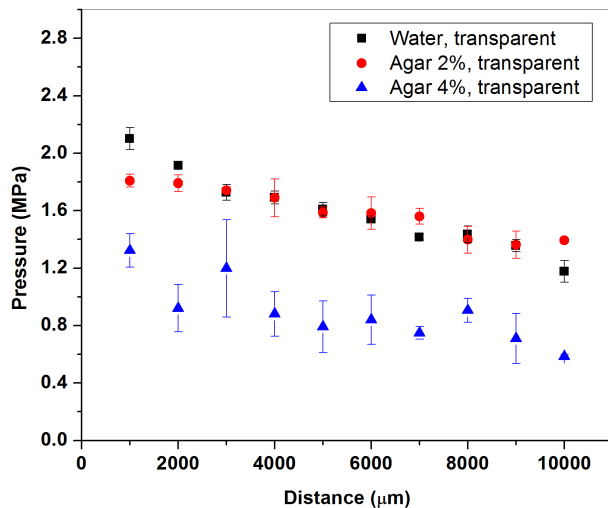


Fig. 4A. Pressure distribution within agar gel from 1 mm to 10 mm measured with PVDF sensor. Energy per pulse was 500 μJ .

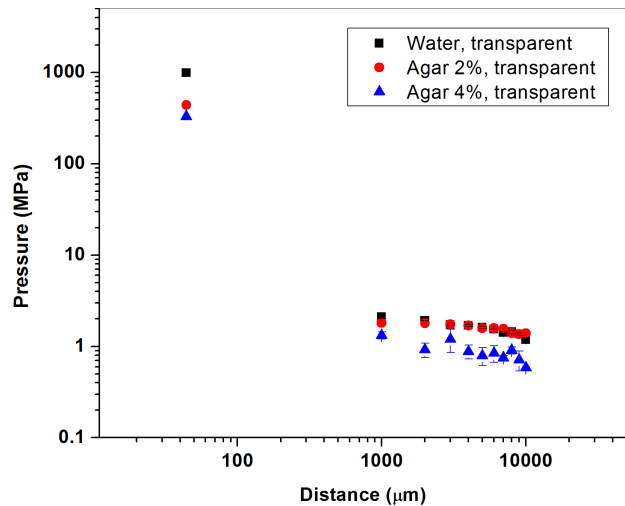


Fig 4B. Pressure distribution within agar gel from 50 μm to 10 mm measured with PVDF sensor and TRI. Energy per pulse was 500 μJ .

3.3 Pressure for different irradiation configurations

Fig. 5A shows the pressure wave originated when an unfocused nanosecond laser pulse is incident on an absorbing agar gel block. The wave gradually increases exponentially with slope according to the Beer's law and its absorption coefficient. If stress confinement conditions are met and ablation threshold is not overcome, the entire signal has a symmetric bipolar shape such that the integral vanishes¹⁰. Fig. 5B shows the typical signal when the beam waist is positioned on the gel surface and Fig. 5C corresponds to the configuration positioning the beam waist 1 mm below the gel surface and. Both signals show a sharp increase at $t = 0$, reach a maximum and then decrease.

In contrast, the sharp rise in Figs. 5B and 5C is produced by a shock wave that is launched due to plasma formation. The pressure signal in Figure 5B shows two spikes on top of the signal originated. In this experiment the beam waist was positioned on the surface of the agar gel using the ETP system previously described, however, there is an inherent error in the beam waist positioning in the order of the lens' Rayleigh range. When the beam waist is positioned 40 μm above the gel surface, twice the Rayleigh range of the lens used, and the irradiance is enough to ionize the air above, two different pressure waves are generated and travel simultaneously. The first, labeled with number 1 in Fig. 5B, is generated by the plasma formation in air and propagates downwards to the sensor. The second spike, labeled with number 2, is originated by linear absorption of the light that propagates after the plasma and is incident on the agar gel surface. The final signal shown in figure 5B is the superposition of these two waves. Interestingly, oscilloscope traces with spikes very similar to those obtained here are shown in recent studies where a PDVF sensor was developed to monitor nanosecond laser induced-bubble collapse near a solid surface^{11, 12}. Clearly the laser exposure configuration used in the present study is very different from that bubble collapse is not the mechanism responsible to produce such spikes in our experiments.

Figure 5C shows a pressure wave originated in an agar gel block when the beam waist was positioned 1 mm below the surface. Here the lower part of the spherical shock wave propagates as a compressive wave towards the sensor, while the upper part propagates also as a compressive wave towards the free surface and is reflected backwards with inverted sign as a tensile wave. The change from compressive to tensile wave takes place due to the acoustic impedance mismatch between the agar gel surface and air. The tensile wave is clearly shown as a sharp decay in the pressure wave in Figure 5C. The time difference between the rise edge of the pulse (compressive) and the fall edge (tensile) agrees well with the time that it takes for an acoustic wave to travel 2 mm at 1500 m/s. For this rough calculation, the deceleration of the wave from shock wave to a pressure wave is neglected.

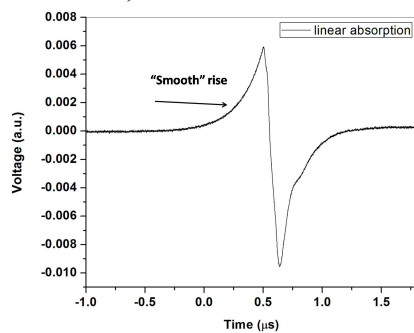


Fig. 5A. Pressure signal obtained with a PVDF sensor when an unfocused, 6 ns laser pulse is incident on an absorbing, 10 mm thick agar gel. $\mu_a=33 \text{ cm}^{-1}$.

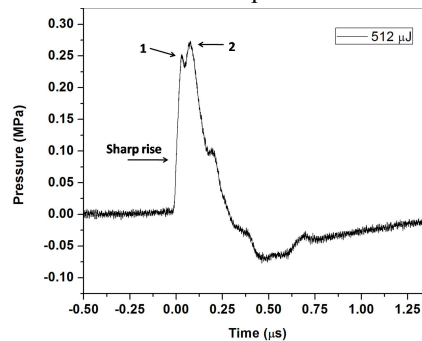


Fig. 5B. Pressure signal obtained with PVDF sensor when a focused, 6 ns laser pulse is incident on an absorbing 10 mm thick agar gel. Beam waist was positioned on the surface of the agar gel. $\mu_a=33 \text{ cm}^{-1}$.

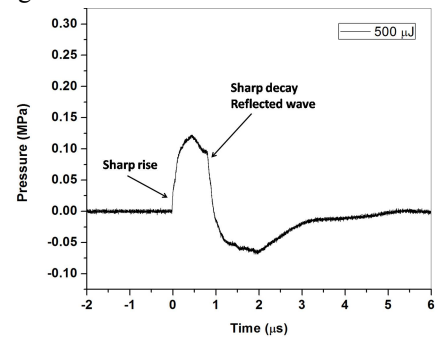


Fig. 5C. Pressure signal obtained with PVDF sensor. Focused, 6 ns laser pulse is incident on absorbing, 10 mm thick agar gel. The beam waist was positioned 1 mm below the agar gel surface. $\mu_a=33 \text{ cm}^{-1}$.

3.4 Linear absorption coefficient

Fig. 6 shows the amplitude of the pressure signals detected with the PVDF sensor when the laser waist was positioned 1 mm below the 2% agar gel surface and 10 mm away from the sensor for different absorption coefficients as a function of the per pulse energy. The transparent agar gel shows higher pressure increments because almost the entire energy from the laser pulse is deposited in the focal volume and is readily available to produce plasma. In contrast, pressure amplitude for absorbing agar gels show lower pressure increments because the beam propagates 1 mm through the gel and the energy that remains to be produce plasma is less than in the previous case. In fact, for the 47 cm^{-1} agar gel blocks, no signal was detected for energies lower than $500\text{ }\mu\text{J}$. The heat generated while the beam propagates through the 1 mm is not enough to induce a pressure wave detectable with the sensor because the size of the beam is large and therefore the fluence low. No changes of the pressue signal as a function of the pulse energy was detected for the configuration when the beam waist was positioned on the surface of the agar gel.

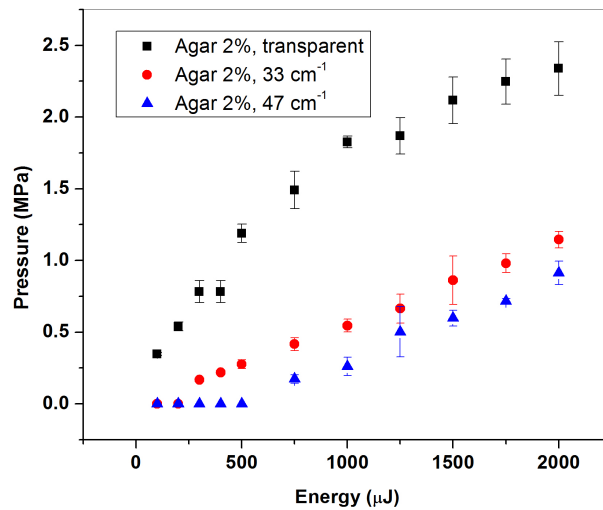


Fig. 6. Pressure amplitude as a function of per pulse energy. Laser pulses were incident 1 mm below the surface of agar gel blocks.

4. CONCLUSIONS

Mechanical effects of irradiation with nanosecond laser pulses of agar gels were studied with mechanical (PVDF) and optical (TRI) means. It was found that the amplitude of the pressure waves detected with a PVDF sensor from 1 to 10 mm away from the beam waist has not significant difference for the agar gel concentrations tested. However the pressure increments a few tens of micrometers from the beam waist are two orders of magnitude higher than 1 mm away; in other words, the pressure amplitude decreases 2 orders of magnitude in the first millimeter of propagation. In addition a brief description of the shape for the pressure signals obtained with the PVDF sensor for the different irradiation configurations was presented. Increasing the linear absorption coefficient of the samples affected the amplitude of the signal when the beam was positioned 1 mm below the surface because plasma formation is weaker due to energy absorbed throughout the 1 mm propagation, which is a clear indication that plasma formation is the dominant interaction mechanism in these experiments. Current research is underway to implement a Mach-Zehnder interferometer to study the relative influence of linear and nonlinear absorption with more sensitivity than the current methods.

5. AKNOWLEDGMENTS

The authors acknowledge Mr. Edgar Arturo Chávez Urbiola for his help with experiments. FGPG thanks CONACyT-UC MEXUS scholarship for graduate studies and UC MEXUS dissertation research grant.

6. REFERENCES

- [1] Oraevsky, A. A., et al., "Plasma mediated ablation of biological tissues with nanosecond-to-femtosecond laser pulses: relative role of linear and nonlinear absorption.," *IEEE Journal of selected topics in quantum electronics* 2(4), 801-809 (1996).
- [2] Vogel, A. and Venugopalan, V., "Mechanisms of pulsed laser ablation of biological tissues," *Chem. Rev.* 103(2), 577-644 (2003).
- [3] Vogel, A., Lauterborn, W., and Timm, R., "Optical and acoustic investigations of the dynamics of laser-produced cavitation bubbles near a solid boundary," *J. Fluid Mech.* 206, 299-338 (1989).
- [4] Brujan, E. A. and Vogel, A., "Stress wave emission and cavitation bubble dynamics by nanosecond optical breakdown in a tissue phantom," *J. Fluid Mech.* 558, 281-308 (2006).
- [5] Evans, R., [Physical phenomena excited in laser-material processing, Ph.D. Thesis], Centro de Investigacion Cientificia y de Educacion Superior de Ensenada, Ensenada, B. C., (2009).
- [6] Viator, J. A., Jacques, S. L., and Prahl, S., "Depth profiling of absorbing soft materials using photoacoustic models," *IEEE Journal of selected topics in quantum electronics* 5(4), 989-996 (1999).
- [7] Perez-Gutierrez, F. G., et al., "Short and ultrashort laser pulse induced bubbles on transparent and scattering tissue models," *Proc. of SPIE*, 64350V1-6435V8 (2007)
- [8] Evans, R., et al., "Pump-probe imaging of nanosecond laser-induced bubbles in agar gel," *Optics Express* 16(10), 7481-7492 (2008).
- [9] Vogel, A., Busch, S., and Parlitz, U., "Shock wave emission and cavitation bubble generation by picosecond and nanosecond optical breakdown in water.," *J. Acoust. Soc. Am.* 100(1), 1996 (1996).
- [10] Paltauf, G. and Dyer, P. E., "Photomechanical Processes and Effects in Ablation," *Chem. Rev.* 103(2), 487-518 (2003).
- [11] Kim, B., et al., "Interferometric analysis of ultrashort pulse laser-induced pressure waves in water," *Journal of Applied Physics* 94(1), 709-715 (2003).
- [12] Kim, B., et al., "Influence of pulse duration on ultrashort laser pulse ablation of biological tissues," *Journal of Biomedical Optics* 6(3), 332-338 (2001).